200730018B

厚生労働科学研究費補助金

こころの健康科学研究事業

終板アセチルコリンエステラーゼ欠損症、及び、他の細胞外マトリックス分子欠損症におけるタンパク標的療法の開発研究

平成17年度～19年度　総合研究報告書

主任研究者　大野　欽司

平成20(2008)年　4月

目　次

I.終板アセチルコリンエステラーゼ欠損症、及び、
他の細胞外マトリックス分子欠損症におけるタンパク標的療法の開発研究

主任研究者　大野　欽司　名古屋大学医学系研究科・神経遺伝情報学・教授
分担研究者　祖父江　元　名古屋大学医学系研究科・神経内科学・教授

研究要旨

先天性筋無力症候群は、神経筋接合部の先天的分子欠損により、顔面・四肢・体幹の筋力低下・筋萎縮・奇形を主徴とする疾患群である。先天性筋無力症候群は、神経筋接合部の先天的分子欠損症が原因であり、主任研究者らは欠損分子に応じた治療法を開発・臨床応用してきた(Engel, Ohno, Sine. *Nat Rev Neurosci* 4: 339, 2003)。しかし、collagen Q分子(*COLQ*遺伝子産物)欠損による終板アセチルコリンエステラーゼ(AChE)欠損症は全く治療法が存在しない(Ohno, et al. *Proc Natl Acad Sci USA* 95: 9654, 1998)。Collagen Q 3分子(*COLQ*遺伝子産物)は3重鎖を形成し、AChE catalytic subunit 12分子と結合し、非対称性A_{12}-AChEを形成する。本研究では、collagen Qがシナプス基底膜への係留シグナルを有する細胞外構造タンパクであることを利用し(Kimbell*, Ohno*, et al. *J Biol Chem* 279: 10997, 2004. *equal contribution)、*COLQ*欠損モデル動物のリンパ球に正常*COLQ*遺伝子と正常*ACHE*遺伝子を導入し、A_{12}-AChEを血中に発現させ、シナプス基底膜への係留を試みた。また、*COLQ*遺伝子導入骨格筋が産生をするA_{12}-AChEが*COLQ*遺伝子非導入骨格筋へ組織間液を介して移行することを期待し、骨格筋への正常*COLQ*遺伝子の導入を行った。

一般に、遺伝子治療においては導入遺伝子の細胞特異的・組織特異的なターゲッティングが障壁となり、培養細胞レベルで有効である手法の多くが臨床応用できない。本研究では、組み替え遺伝子を標的組織にターゲッティングさせる代わりに、欠損タンパクが細胞外分子であることと、タンパクに標的組織親和性があることを利用して標的組織へのターゲッティングを行う。本手法は、他の神経難治疾患であるperlecan欠損症、collagen I欠損症、α_2 laminin欠損症、α dystroglycanopathyを含む細胞外マトリックスタンパク欠損症一般への応用の可能性が期待される。

また、先天性筋無力症候群は、世界中からおよそ200例が報告されており、7種類の神経筋接合部分子において約180種類の遺伝子変異が同定されてきている。これらのうちファウンダー効果が明らかなものは*RAPSN*遺伝子における1変異のみであり、他の多くの遺伝子変異は個々の家系に特有の遺伝子変異か、de novo遺伝子変異であり、人種や地域を問わず本症候群が存在すると想定されるが、わが国からの報告は極めて稀である。本研究では、本症候群の診断に反復神経刺激が有用であることを利用し、筋力低下を主徴とする非定型的な神経筋疾患に対して積極的に反復神経刺激を行い、スローチャンネル症候群の一例を同定し、その治療効果について検討を行った。

A. 研究目的

神経筋接合部の分子欠損症による先天性筋無力症候群は、世界中から数多くの症例が報告されているが日本からの報告は少ない。諸外国でも*de novo*遺伝子変異が数多く存在することから、本症候群は日本にも多数存在すると考えられる。胎生期からの神経筋接合部伝達障害によると思われる小奇形、筋萎縮、関節拘縮がみられ、諸外国で見られるように日本でも筋ジストロフィー症や先天性筋症と診断をされている例が少なからず存在すると思われる。また、重症筋無力症と診断をされ、不必要な胸腺摘出術や免疫抑制療法を受けている症例も、諸外国同様に日本にも数多く存在すると思われる。先天性筋無力症候群は欠損分子に応じた治療が可能であるタイプが多く、本症候群の診断、及び新規治療法開発研究は、患者利益につながると期待をされる。

本研究においても、軽度四肢近位筋力低下・労作性呼吸困難・複視を伴わない幼少時からの斜視を主徴とする37歳男性がアセチルコリン受容体βサブユニットのV296A変異を有するスローチャンネル症候群であることを同定した。

先天性筋無力症候群の中でも、*COLQ*遺伝子変異による終板AChE欠損症は、従来、全く治療法が存在しない。わが国の終板AChE欠損症の一例も不幸な転帰を辿っている。本研究では、終板AChE欠損症に対して、臨床応用を近視野に入れたタンパク標的療法の開発研究を行う。本研究にて開発する手法は、神経難治疾患を含む他の細胞外マトリックスタンパク欠損症への応用の可能性がある。

B. 研究方法

Collagen Q（*COLQ*遺伝子産物）は、コラーゲンドメインを介して3分子が3重鎖構造を形成し、acetylcholinesterase (AChE) catalytic subunit（*ACHE*遺伝子産物）12分子と結合し、非対称性A_{12}-AChEを形成する。本研究では、collagen Qがシナプス基底膜への係留シグナルを有する細胞外構造タンパクであることを利用し、*COLQ*欠損モデル動物のTリンパ球に正常*COLQ*遺伝子と正常*ACHE*遺伝子を導入し、A_{12}-AChEを血中に発現させ、シナプス基底膜への係留を試みた。また、骨格筋に*COLQ*遺伝子を導入し、一部の骨格筋に発現したA_{12}-AChEが、血流・組織間液を介して*COLQ*遺伝子非導入骨格筋のシナプス基底膜への係留することを確認した。

I. *ColQ*欠損マウスの評価

ヘテロの*ColQ*欠損マウス(フランスINSERMのDr. Eric Krejci より譲渡)を交配し、そこから産まれた*ColQ*+/+, *ColQ*+/-, *ColQ*-/-マウスの表現型について評価を行う。運動機能を調べるため、ロタ・ロッド試験を行う。4分間で0～40 rpmまで加速回転する棒上で、マウスが乗り続けられる時間を計測する。また、*ColQ* +/+, *ColQ* +/-, *ColQ* -/-マウスの筋肉組織中のAChEの分子形状をショ糖濃度勾配遠心法を用いて調べる。

II. レトロウィルスベクターの構築

レトロウィルスベクターを用いて、モデルマウスにヒト*COLQ*遺伝子を導入、発現させる手法の確

立を試みる。レトロウィルスベクターpSIREN-RetroQ (Clontech社)に、リンパ球系細胞で活性が高いEF1αプロモーターを組み込み、その下流にヒト*ACHE* cDNA・IRES・ヒト*COLQ* cDNAを組み込む。*COLQ*欠損モデル動物のTリンパ球に遺伝子導入を行う。目的組織へのターゲッティングはColQがシナプス基底膜への係留シグナルを有する細胞外構造タンパクであることを利用する。正常ヒト*ACHE*遺伝子と正常ヒト*COLQ*遺伝子を導入する。このレトロウィルスをパッケージング細胞PLAT-Eに導入し、産出させた組み換えレトロウィルスをNIH 3T3細胞に感染させ、A_{12}-AChEの細胞内発現及び細胞外放出を確認する。

III. マウスリンパ球へのレトロウィルスの導入及びマウスへの注入

正常マウスの脾臓、リンパ節よりCD3及びCD28抗体を用いてTリンパ球を単離する。IL2の存在下に培養を行い、上記レトロウィルスを感染させる。次に、細胞培養液中の組み替えA_{12}-AChEをヘパリンアガロースカラムで精製を行い、ショ糖濃度勾配遠心法により分離し、形質転換Tリンパ球が、組み替えA_{12}-AChEを合成し培養液中に放出することを確認する。その後、形質転換Tリンパ球を正常マウスに注入する。

IV. AAV (adeno-associated virus)を用いた*COLQ*遺伝子導入

AAVベクターは、神経・筋・肝細胞等の非分裂細胞に対し一回の導入で長期的な遺伝子発現が得られ、また安全性の点でも非病原性・低免疫原性など他のウイルスベクターに比べ利点が多い。ここでは筋肉組織への親和性が高いserotype 8を選び用いる。AAVベクターは、pAAV-CMV-MCS (Stratagene社)を用いて、骨格筋において高活性を示すCMV promoterの下流に*COLQ*を挿入したコンストラクトを作製する。AAVベクターをヘルパーベクターpDF6と共にリン酸カルシウム法によりHEK293T細胞にトランスフェクションし、得られたrAAVウィルス粒子をAAVHT1080に感染させ、GFP発現細胞をフローサイトメトリーを用いて測定し、細胞への遺伝子導入効率を調べる。

V. 治療マウスの評価

ヒトAChEに対するモノクローナル抗体(米国Mayo Clinic, Dr. Andrew G. Engelより供与)とヒトColQに対するポリクローナル交代を用いて、治療マウスのシナプス基底膜における組み換えA_{12}-AChEの発現を調べる。また、AChE活性染色を用いて同様の検討を行う。さらに、ショ糖濃度勾配遠心法によるAChE分画により、A_{12}-AChE分子の骨格筋における発現を調べ、微小終板電位の減衰時間を測定することにより神経接合部におけるAChE補充量を類推する。さらに、腎糸球体基底膜や中枢神経系への異所性のColQ発現を調べる。

C. 研究結果

I. レトロウィルスベクターを用いた *COLQ* 遺伝子と *ACHE* 遺伝子の導入

Clontech社のpSIREN-RetroQベクターを改変して、EF1αの下流にヒト*ACHE*遺伝子,

IRES,*COLQ*遺伝子を導入し、p-SIREN-EF1α-*ACHE*-IRES-*COLQ*, p-SIREN-EF1α-*ACHE*, pSIREN-EF1α-*COLQ*を構築した。作製したベクターを、PLAT-E細胞にトランスフェクションをし、組換えレトロウィルスを得た。組換えレトロウィルスをNIH3T3細胞に感染させ、タンパクの発現を確認した。*ACHE*-IRES-*COLQ*単独、及び、*ACHE*と*COLQ*の同時感染させたNIH3T3細胞において、その細胞内と培地中に放出されたAChEをショ糖濃度勾配遠心法で分画しAChEのformを調べた。どちらのレトロウィルス感染の場合も、G_1, G_2, G_4-formsに加えA_4, A_8, A_{12}-formsの活性が細胞内だけでなく、培地中でも検出された。感染により細胞内に導入をしたColQとAChEがA_4, A_8, A_{12}-formsの複合体を形成し、細胞外に放出されていることを示している。

II.マウスリンパ球へのレトロウィルスの導入及びマウスへの注入

正常マウスから脾臓・リンパ節を摘出し、血球をCD3及びCD28抗体存在下で培養してTリンパ球の単離を行ない、Tリンパ球の増殖の良好な培養系を確立した。T-cellに組換えレトロウィルスを感染させ、２日間培養後、細胞内と培地中のAChE formを調べた。いずれにおいて、A_4, A_8, A_{12}-formsが検出され、組換えTリンパ球により形成されたColQとAChEの複合体が細胞外に移行することを確認した。

現在、大量のTリンパ球の単離、及びレトロウィルスの生産を行い、マウス生体内に注入できる量の遺伝子導入Tリンパ球を作製している。今後、この組換えTリンパ球を正常マウスに静脈注射する。ヒトAChEに対するモノクローナル抗体を用いて、組み換えA_{12}-AChEの血中での発現を調べ、さらに、シナプス基底膜への係留の有無を調べる。良好な結果が得られた後、*ColQ*-/-マウスに適用し、非対象性A_{12}-AChE分子の発現、及び、神経接合部でのA_{12}-AChE分子の集積、生理学的・形態学的検査を行い、筋無力症状の機能回復・安全性について検討する。

III. AAV (adeno-associated virus)を用いた*COLQ*遺伝子導入

AAVベクターはpAAV-CMV-*COLQ*と、ColQと共にGFPを発現するpAAV-CMV-*COLQ*-IRES-*EGFP*のコンストラクトを作成した。AAV8型カプシドをコードするヘルパープラスミドと同時にHEK293細胞に導入し、rAAV8-ColQとrAAV8-ColQ-EGFPの２種類の組み替えAAVを作製した。強イオン膜を用いて精製した後、*ColQ*-/-マウスの尾静脈より全身投与（2×10^{11} genome copies）を行った。

投与2週間後から、ロタロッドでの運動テストに改善効果が見られ、４週間後には、運動テストと疲労テストで正常マウスと同成績まで回復した。治療マウスの骨格筋組織切片のAChE活性染色にて、αバンガロトキシンで染まるアセチルコリンレセプターと同一の部位に、AChE活性が見られた。また、ColQ抗体による免疫染色においても、同じ部位でシグナルが検出され、神経筋接合部においてColQが集積していることが確認できた。さらに、ショ糖勾配遠心法により、治療マウスの骨格筋中のAChE-formを検出したところ、未治療群では

見られなかったA_4, A_8, A_{12}-formsのAChEが検出された。さらに、治療マウスの微小終板電位の減衰時間は正常マウスとノックアウトマウスの中間の値となり、A_{12}-AChEの発現は正常量までは回復をしていないと予想された。しかし、治療マウスの運動機能がほぼ正常化したことは、神経筋信号伝達の安全域を超える程度までA_{12}-AChEの発現量が回復をしたと考えられた。以上の結果から、AAV8を介して*COLQ*の遺伝子導入により、発現したColQがAChEと複合体を形成し神経筋接合部に係留すること、また治療マウスは、運動機能テストから筋無力症状が正常値まで回復したことが明らかになった。ColQは基底膜に係留シグナルを持つ細胞外タンパクであるため、遺伝子導入された骨格筋細胞の割合が低くても、自らの細胞外標的シグナルにより、十分量のA_{12}-AChEが神経筋接合部に移行をした考えられた。治療後最高３ヶ月間の観察では、改善した運動機能の再増悪もなく、また、神経筋接合部へのリンパ球浸潤もなく、良好な経過を辿っている。今後、筋無力症状の機能回復が可能なウィルス投与量の最低値の決定、組換えA_{12}-AChEの腎糸球体基底膜などへの異所性集積や抗collagen Q抗体の出現など、遺伝子導入の安全性を検討して行く予定である。

IV. スローチャンネル症候群の検討

36歳発症の軽度四肢近位筋力低下と労作性呼吸困難を主訴とする37歳男性がスローチャンネル症候群であることを見出し、薬剤による治療が極めて有効であることを見出した。患者は、幼少時からの斜視があるが複視を訴えない。診察時に易疲労性を認めず、日内変動もなく、edrophoniumテストも陰性であり、重症筋無力症を含む神経筋接合部疾患を積極的に疑う臨床所見に欠けている。単発神経刺激にて2発の反復CMAPを認めた。反復CMAPは、(1) スローチャンネル症候群、(2) 終板acetylchoinesterase欠損症、(3) 抗cholinesterase剤や有機リン中毒によるacetylcholinesterase活性抑制で認められる。脛骨神経の3 Hzの反復神経刺激にて22%の異常減衰を認め、 single fiber EMGではMCDが98 ± 54μsと延長しており、神経筋接合部信号伝達の異常が示唆された。

AChRサブユニット遺伝子変異によるスローチャンネル症候群と、collagen Q遺伝子変異による終板acetylcholinesterase欠損症を疑い、網羅的な遺伝子変異の検索を行ったところ、AChR βサブユニットにV296A変異を認めた。患者は正常alleleと変異alleleを持つheterozygoteであり、βV296Aはドミナント変異であった。

βV296は第3膜貫通ドメインほぼ中央部に位置し、αサブユニットで対応するアミノ酸はαV285である。イオンチャンネルの開口時間が異常に短縮するファーストチャンネル症候群においてαV285I変異が報告されている(Wang H-L, Milone M, Ohno K, et al. *Nat Neurosci* 2: 226, 1999)。αV285I変異の研究において、αV285L、αV285I、αV285T、αV285Aの4種類の変異αサブユニットの解析が行われており、コドン285におけるアミノ酸側鎖のボリュームが、イオンチャンネルの動態を決定していることが判明している。つまり、valineよりもボリュームが大きいleucineやisoleucineではファーストチャンネルとなり、valineよりもボリュームが小さいthreonineやalanineではスローチャンネルとなる。この事実は、第3膜貫通ドメインほぼ中央部のコドン285におけるアミ

ノ酸側鎖が、AChRのチャンネル孔を形成する第2膜貫通ドメインを背側から押していることを示している。AChR α, β, δ, εサブユニットは相同なサブユニットであり、第3膜貫通ドメインのβV296Aは第2膜貫通ドメインを背側から押す力を弱め、AChRのチャンネル孔を開きやすくさせるスローチャンネル変異と想定され、事実、単一チャンネル記録にてチャンネル開口が異常に遅延していることを実験的に証明した。

イオンチャンネルブロッカであり、スローチャンネル症候群に対する有効性が確立しているquinidine常用量(400 mg/day)を投与したところ、四肢筋力が改善し、反復神経刺激に対するCMAPの異常減衰も軽減し、単発神経刺激に対する反復CMAPも軽減した。しかし、寒冷誘発性のアセチルコリン放出効率の低下とAChR開口効率の低下によると思われる寒冷時の四肢筋力低下と呼吸不全を認めたため、fluoxetine常用量(40 mg/day)を追加し、さらなる四肢筋力の改善を認めた。

D. 考察

本研究において、レトロウィルスのTリンパ球への導入と、組換えA_{12}-AChEのTリンパ球から培養液中への放出を確認した。A_{12}-AChEは正常においては骨格筋細胞から放出され、神経筋接合部に係留するるが、COS細胞やHEK293細胞など繊維芽細胞系からも放出されることが知られてきた。本研究で、Tリンパ球もA_{12}-AChEを放出することが判明し、リンパ球を用いたタンパク標的療法の開発研究を進めて行きたい。今後は、大量の遺伝子組換えTリンパ球の調整方法を確立し、モデル動物の治療を行う予定である。

骨格筋への親和性を有するAAV8を用いた研究では、モデル動物の治療に成功した。5週齢のマウスに治療を行い、運動機能がほぼ正常化できたことは、本プロジェクトで提案をしてきた「タンパク自体の組織親和性を用いたタンパク標的療法」の有用性を示唆している。

また、未診断の先天性筋無力症候群の同定を今後とも積極的に行って行きたい。今回解析を行った症例に見られるように先天性筋無力症候群の中には、成人発症で、日内変動を伴わず、易疲労性も明らかでない症例が多く存在すると思われる。本症例も、呼吸筋が優位に侵され、明らかな易疲労性を認めず、鑑別診断として重症筋無力症や先天性筋無力症候群を考えにくい臨床像であった。本症例でも、単発神経刺激による反復CMAPの出現と、反復神経刺激におけるCMAP電位の異常減衰が診断に有用であり、筋力低下を主徴とする神経疾患に対して電気生理学手法を用いた神経筋接合部欠損の検索を行う重要性が示唆された。

E. 結論

タンパク標的療法は従来の神経筋疾患モデル動物の遺伝子治療ではみられない程度の良好な運動能力改善効果を示した。今後、本手法の臨床応用や他疾患への応用を含めて研究を行って行きたい。

先天性筋無力症候群は、スローチャンネル症候群をはじめとして病態に応じた治療方法が可能な疾患群が多く、本症候群に対して積極的に電気生理学診断を行う重要性が示された。

F. 健康危険情報

特記事項なし。

G. 研究発表

1. 論文発表

1. Ohno K, Tsujino A, Shen X-M, Milone M, Engel AG. Spectrum of splicing errors caused by *CHRNE* mutations affecting introns and intron/exon boundaries. *J Med Genet* 2005, 42: e53.
2. Shen X-M, Ohno K, Sine SM, Engel AG. Subunit-specific contribution to agonist binding and channel gating revealed by inherited mutation in muscle acetylcholine receptor M3-M4 linker. *Brain* 2005, 128:345-355.
3. Ito M, Masuda A, Jinno S, Katagiri T, Krejci E, Ohno K. Viral vector-medicated expression of human collagen Q in cultured cells. *Chemico-Biological Interactions* 2008, in press.
4. Shen X-M, Fukuda T, Ohno K, Sine SM, Engel AG. Novel AChR δ subunit mutation causing myasthenia hinders intersubunit link essential for channel gating. *J Clin Invest* 2008, in press

2. 学会発表

1. Ito M, Masuda A, Jinno S, Katagiri T, Krejci E, Ohno K. Gene Therapy for Collagen Q defects in congenital myasthenic syndromes. The IXth International Meeting on Cholinesterases, Shuzou, China. May 10, 2007

H. 知的財産権の出願・登録状況

特記事項なし。

II. 研究成果の刊行に関する一覧表

発表者名	論文タイトル名	発表誌名	巻号	ページ	出版年
Ohno K, Tsujino A, Shen X-M, Milone M, Engel AG	Spectrum of splicing errors caused by *CHRNE* mutations affecting introns and intron/exon boundaries	*J Med Genet*	42	e53	2005
Shen X-M, Ohno K, Sine SM, Engel AG	Subunit-specific contribution to agonist binding and channel gating revealed by inherited mutation in muscle acetylcholine receptor M3-M4 linker	*Brain*	128	345-355	2005
Ito M, Masuda A, Jinno S, Katagiri T, Krejci E, Ohno K	Viral vector-medicated expression of human collagen Q in cultured cells	*Chemico-Biological Interactions*		in press	2008
Shen X-M, Fukuda T, Ohno K, Sine SM, Engel AG	Novel AChR δ subunit mutation causing myasthenia hinders intersubunit link essential for channel gating	*J Clin Invest*		in press	2008

Spectrum of splicing errors caused by CHRNE mutations affecting introns and intron/exon boundaries

K Ohno, A Tsujino, X-M Shen, M Milone and A G Engel

J. Med. Genet. 2005;42;53-
doi:10.1136/jmg.2004.026682

ONLINE MUTATION REPORT

Spectrum of splicing errors caused by *CHRNE* mutations affecting introns and intron/exon boundaries

K Ohno, A Tsujino, X-M Shen, M Milone, A G Engel

J Med Genet 2005;**42**:e53 (http://www.jmedgenet.com/cgi/content/full/42/8/e53). doi: 10.1136/jmg.2004.026682

Background: Mutations in *CHRNE*, the gene encoding the muscle nicotinic acetylcholine receptor ε subunit, cause congenital myasthenic syndromes. Only three of the eight intronic splice site mutations of *CHRNE* reported to date have had their splicing consequences characterised.
Methods: We analysed four previously reported and five novel splicing mutations in *CHRNE* by introducing the entire normal and mutant genomic *CHRNE*s into COS cells.
Results and conclusions: We found that short introns (82–109 nucleotides) favour intron retention, whereas medium to long introns (306–1210 nucleotides) flanking either or both sides of an exon favour exon skipping. Two mutations are of particular interest. Firstly, a G→T substitution at the 3′ end of exon 8 predicts an R286M missense mutation, but instead results in skipping of exon 8. In human genes, a mismatch of the last exonic nucleotide to U1 snRNP is frequently compensated by a matching nucleotide at intron position +6. *CHRNE* intron 8 has a mismatch at position +6, and accordingly fails to compensate for the exonic mutation at position −1. Secondly, a 16 bp duplication, giving rise to two 3′ splice sites (g.IVS10-9_c.1167dup16), results in silencing of the downstream 3′ splice site. This conforms to the scanning model of recognition of the 3′ splice site, which predicts that the first "ag" occurring after the branch point is selected for splicing.

Molecular defects of presynaptic, synaptic, or postsynaptic proteins at the motor endplate impair neuromuscular transmission and result in congenital myasthenic syndromes (CMS).[1] Mutations in the acetylcholine receptor (AChR) ε subunit gene (*CHRNE*; OMIM 100725) cause endplate AChR deficiency and/or kinetic abnormalities of AChR. *CHRNE* mutations causing endplate AChR deficiency include 13 missense, 27 frameshift, 6 nonsense, 8 splice site, 3 promoter region, and 1 chromosomal microdeletion mutations.[1] Only three of the eight splice site mutations have had their consequences characterised: IVS7-2A→G[2] and IVS9+1G→T[3] result in skipping of an adjacent exon, and IVS9-1G→C causes retention of intron 9.[4] Four of the five uncharacterised mutations were reported by us. Exclusive expression of *CHRNE* by subsynaptic nuclei has previously prevented analysis of splicing consequences of these mutations. We recently reported that the cloned entire *CHRNE* exhibits the same splicing properties as its pre-mRNA in the native state in transfected COS cells.[4] Therefore we used this method to analyse the splicing consequences of four previously reported and five novel splice site mutations in *CHRNE*.

MATERIALS AND METHODS

All human studies were in accord with the guidelines of the institutional review board of the Mayo Clinic.

Patients

Patients 1–5 (respectively a 59 year old woman, a 23 year old man, a 2.5 year old girl, a 6 year old boy, and a 44 year old man) have moderate to severe myasthenic symptoms that have been present since birth or infancy, decremental EMG responses, and no AChR antibodies. All respond partially to pyridostigmine. Patient 4 underwent an intercostal muscle biopsy for diagnosis, which showed severe endplate AChR deficiency (6% of normal) and compensatory expression of the fetal γ-AChR at the endplate.

Construction of *CHRNE* clones for splicing analysis

To examine the consequences of the identified splice site mutations, we used the previously constructed pRBG4-*CHRNE* plasmid, which carries a cytomegalovirus (CMV) promoter and the entire *CHRNE* spanning 12 exons and 11 introns.[4] For extended analysis of g.IVS10-9_c.1167dup16, we also constructed a pRBG4 minigene, spanning nucleotide 880 in exon 9 to nucleotide 1457 in exon 12, where position +1 represents the first nucleotide of the first codon of the mature peptide.

Mutations were engineered using the QuikChange Site Directed Mutagenesis kit (Stratagene). Presence of the expected mutation and absence of unwanted artefacts were confirmed by sequencing the entire insert.

Reverse transcription PCR analysis of cytoplasmic RNA of transfected COS cells

Wild type and mutant *CHRNE* clones were introduced into COS-7 cells, and cytoplasmic total RNA was isolated as described.[4] We used two or more sets of PCR primers for each construct to screen for skipping of an exon and retention of an intron.

RESULTS

Each patient carries two mutant *CHRNE* alleles

We detected a total of seven *CHRNE* mutations in five patients (table 1). Patients 1, 2, and 3 carry homozygous splice site mutations. Five mutations affect pre-mRNA splicing. Analysis of family members reveals that affected siblings carry two mutant *CHRNE* alleles, whereas unaffected relatives harbour one or no mutant allele (data not shown), indicating that each mutation is recessive.

Splicing consequences of five novel and four previously reported mutations

Muscle mRNA was available only from patient 4. In this patient, RT-PCR analysis revealed that 1259del23 causes retention of intron 11 (fig 1, table 1). As no muscle specimens were available from the other patients for mRNA analysis, we introduced the four novel (table 1) and the four previously reported (table 2) splice site mutations into the cloned entire *CHRNE* and analysed the cytoplasmic RNA of the transfected COS cells by RT-PCR. Unlike minigenes, entire *CHRNE* clones mostly yielded a single splicing product. RT-PCR analysis revealed that IVS4-2A→C, IVS6+1G→T, IVS10+2T→G, and

Table 1 Five splicing, one frameshift, and one missense mutations in *CHRNE* in the five patients

No.	Mutation	Position on genomic DNA	Splicing consequence
1	g.IVS6-1G→C*	3′ splice site of intron 6	Active cryptic 3′ splice site†
2	g.IVS9-1G→A*	3′ splice site of intron 9	Retention of intron 9† Skipping of exon 10†
3	g.IVS10-9_c.1167dup16*	16 bp duplication comprising 8 bp at 3′ end of intron 10 and 8 bp at 5′ end of exon 11	Silencing of downstream 3′ splice site†
4	c.1259_g.IVS11+15del23	23 bp deletion comprising 8 bp at 3′ end of exon 11 and 15 bp at 5′ end of intron 11	Retention of intron 11‡
	c.1033delG	exon 10 (61st nucleotide)	NA
5	c.857G→T (p.R286M)	G→T substitution at 3′ end of exon 8	Skipping of exon 8†
	c.734C→T (p.P245L§)	exon 7 (193rd nucleotide)	NA

*Homozygous mutation. †Characterised using transfected COS cells. ‡Characterised using muscle mRNA. NA, not applicable. §We previously reported that P245L is a low expressor mutation that also prolongs channel opening events two fold.[15]

857G→T cause skipping of an adjacent exon; IVS7+2T→C and 1259del23 result in retention of the mutant intron; IVS9-1G→A causes both exon skipping and intron retention; IVS6-1G→C activates a cryptic 3′ splice site; and g.IVS10-9_c.1167dup16 silences the downstream copy of the 3′ splice site (fig 1, tables 1 and 2).

Why is the downstream copy of duplicated 3′ splice sites silent?

The 16 bp duplication (g.IVS10-9_c.1167dup16) generates two copies of 3′ splice sites, but only the upstream copy is used for splicing. To understand the underlying mechanism, we engineered a series of artificial mutations into a minigene spanning *CHRNE* exons 9 to 12 (fig 2A and B).

Firstly, we examined a role of the polypyrimidine tract of the upstream and downstream copies (fig 2C). The pyrimidine ratios in the polypyrimidine tract are the same for the two copies (18/24 = 75% for the upstream copy and 30/40 = 75% for the downstream copy), and are not likely to account for selection of the splice site. Substitution of "ac" for the invariant "ag" dinucleotide of the upstream copy activated the downstream copy (Mt-AC in fig 2D), indicating that the increased distance from the branch point to the "ag" dinucleotide does not hinder splicing. Because a stretch of t bases in the polypyrimidine tract is more efficient in splicing than c bases,[5] we mutated "cctt" to "tctt" (Mt-TC), "cttt" (Mt-CT), and "tttt" (Mt-TT), but none activated the downstream copy (fig 2D).

The role of the branch point sequence was then examined. Displacement of an invariant "a" nucleotide downstream (Mt-Br1 in fig 2E), disruption of the native branch point sequence (Mt-Br2 in fig 2E), or both (Mt-Br3 in fig 2E) had no effect on splicing. Preserved splicing even in the absence of the branch point consensus sequence CURAY in Mt-Br2 indicates that an "a" residue somewhere in intron 10 serves as a branch point, and confirms that the position and context of the branch point sequence is degenerative in mammals.

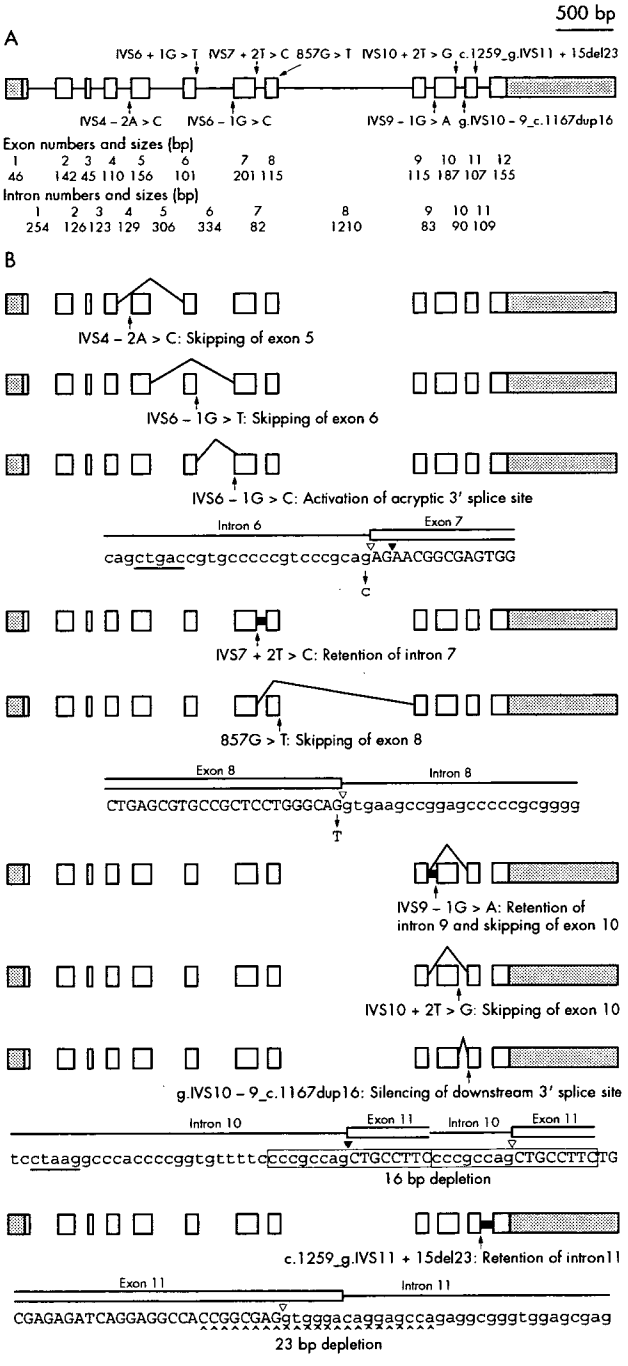

Figure 1 Nine analysed *CHRNE* mutations affecting pre-mRNA splicing. (A) The *CHRNE* gene structure is drawn to scale. Shaded areas indicate untranslated regions. Sizes of exons 1 and 12 represent those of the coding regions. (B) Schematic presentation of identified splicing consequences. Exon skipping and activation of a cryptic splice site are represented by thin oblique lines connecting two remote points. Intron retention is represented by a thick horizontal line. Four splicing mutations are shown in detail, with partial *CHRNE* sequence below each scheme. Open and closed arrowheads indicate inactive and active splice sites, respectively. Putative branch point sequences are underlined.

We next swapped the seven residue segments and placed the native branch point sequence 16 residues downstream (Mt-Br4 in fig 2E). Mt-Br4 activated both the upstream and downstream copies of the 3′ splice sites, probably because the shortened polypyrimidine tract rendered the upstream copy of the splice acceptor site less competitive than the downstream copy.

Table 2 Four previously reported splice site mutations in *CHRNE*

Mutation	Position on genomic DNA	Splicing consequence
g.IVS4-2A→C[4]	3′ splice site of intron 4	Skipping of exon 5
g.IVS6+1G→T[19]	5′ splice site of intron 6	Skipping of exon 6
g.IVS7+2T→C[20]	5′ splice site of intron 7	Retention of intron 7
g.IVS10+2T→G[21]	5′ splice site of intron 10	Skipping of exon 10

DISCUSSION

Sizes of flanking introns predict exon skipping or intron retention

We analysed splicing consequences of nine mutations in *CHRNE*. Three other splicing mutations had been previously characterised.[2–4] To summarise, exons 5, 6, 8, 9, and 10 are skipped, and introns 7, 9, and 11 are retained. The three retained introns are all short (intron 7, 82 bp; intron 9, 83 bp; and intron 11, 109 bp), whereas four of five skipped exons flank medium to long introns on either or both sides (exon 5 is flanked by 129 and 306 bp introns; exon 6 by 306 and 334 bp introns; exon 8 by 82 and 1210 bp introns; and exon 9 by 1210 and 83 bp introns). This is in accordance with collation of splicing mutations,[6] and is consistent with the model of exon recognition in vertebrate splicing.[7] Exon 10, however, is flanked by 83 and 90 bp introns, and is skipped by two distinct mutations, indicating that the size of the flanking introns is only one of several factors that determine the splicing consequence. Indeed, even when we eliminated 1127 bp in the middle of intron 8 (IVS8+17 to IVS8-59) to reduce its size to 83 bp, both IVS7-2A→G and 857G→T still resulted in skipping of exon 7 (data not shown).

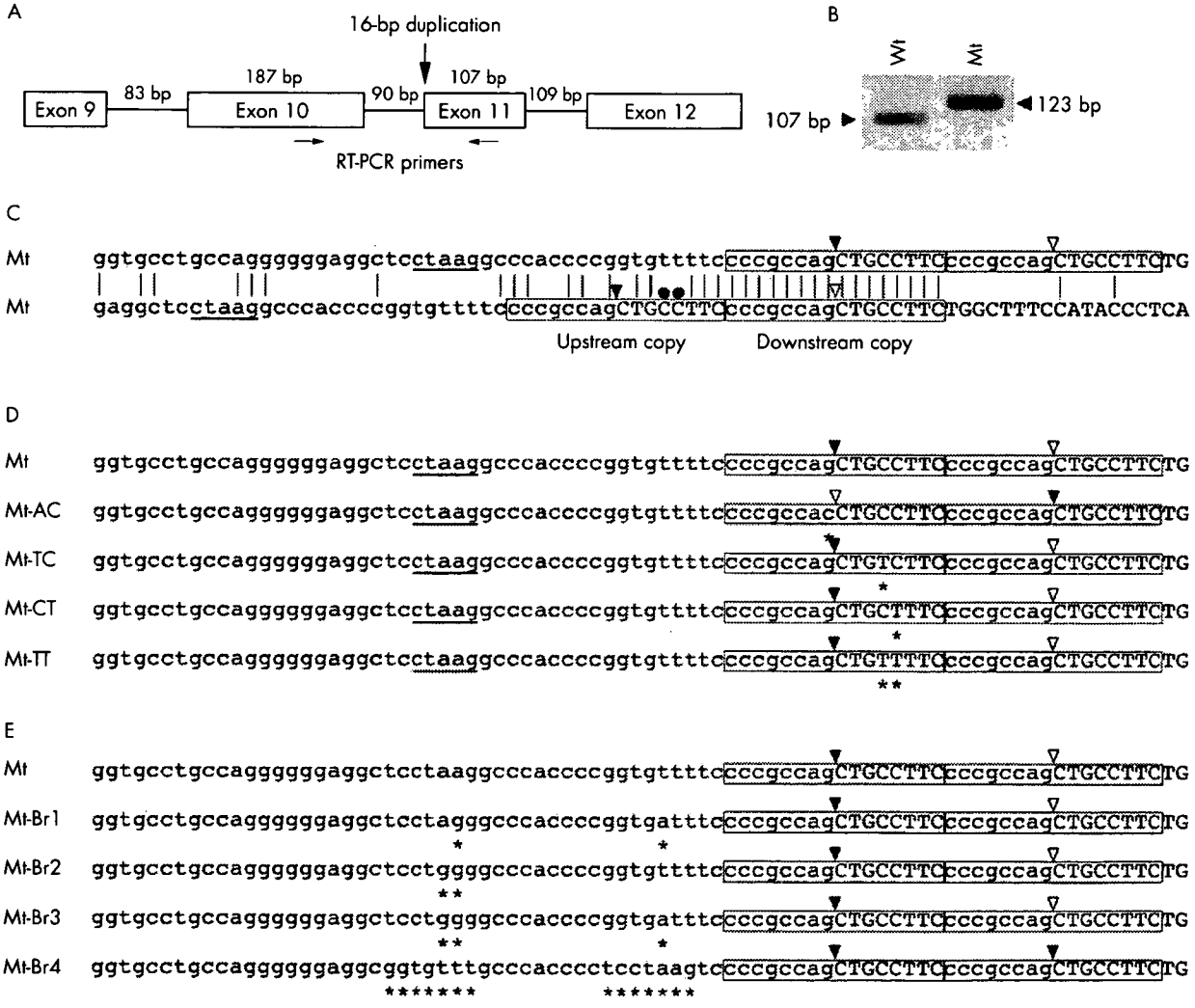

Figure 2 A 16 bp duplication of the 3′ splice site of *CHRNE* intron 10/exon 11 boundary results in silencing of the downstream copy of the 3′ splice sites by competition against the upstream copy. (A) A minigene spanning exons 9–12, which is inserted into a CMV based expression vector. (B) RT-PCR analysis of cytoplasmic RNA of transfected COS cells shows that only the upstream copy of the splice acceptor site is active. (C) Alignment of active (closed arrowhead) and inactive (open arrowhead) 3′ splice sites of the mutant (Mt) intron 10/exon 11 boundary. The two sequences are identical, but are shifted by 16 bp. Vertical lines indicate identical nucleotides. Duplicated 3′ splice sites are enclosed by boxes. Putative branch point sequence (CTRAY with an invariant A) is underlined. Upper and lower case letters represent exonic and intronic nucleotides, respectively. Dots point to mismatches that are corrected in Mt-TC, Mt-CT, and Mt-TT in panel D. (D) Disruption of an "ag" dinucleotide in the upstream copy activates the downstream copy (Mt-AC), whereas partial (Mt-TC and Mt-CT) or complete (Mt-TT) restoration of a "ttt" stretch in the polypyrimidine tract has no effect. Closed and open arrowheads point to active and inactive 3′ splice sites, respectively. Asterisks indicate artificially mutated nucleotides. (E) Partial displacement of the native branch point (Mt-Br1), disruption of the branch point (Mt-Br2), or both (Mt-Br3) fails to activate the downstream copy of the duplicated 3′ splice sites, whereas swapping of the seven residue segments (Mt-Br4) activates both the upstream and downstream copies.

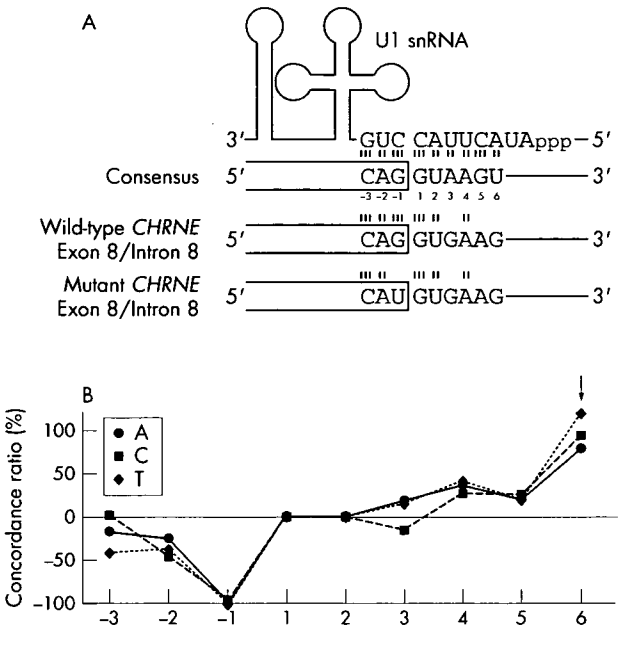

Figure 3 (A) U1 snRNA recognises three nucleotides at the 3′ end of an exon and six nucleotides at the 5′ end of an intron. The complementary nucleotides to U1 snRNA constitute the consensus sequence. Wild type *CHRNE* exon 8/intron 8 has mismatched nucleotides at positions +3, +5, and +6. The 857G→T mutation introduces another mismatch at position −1. (B) A mismatch at the last nucleotide of an exon (position −1) to U1 snRNA is mostly compensated for by a match at position +6 in 1801 human exons. The ratios of A, C, G, and T at position −1 are 8.8%, 3.3%, 80.3%, and 7.5%, respectively, in 1801 human exons.[17] When a concordant G is used at position −1, the ratio of concordant T at position +6 is 38.9%. In contrast, when a discordant T is used at position −1, the ratio of concordant T at position +6 is 85.9%. The concordance ratio was calculated by (85.9–38.9)/38.9 = 121% (arrow). A positive concordance ratio at a specific position indicates that a nucleotide complementary to U1 snRNA is preferentially used to compensate for a mismatch at position −1.

Why does a mutation at the 3′ end of an exon affect pre-mRNA splicing?

Analysis of 1801 human 5′ splice sites[17] revealed that a mismatch at position −1 to U1 snRNA is mostly compensated for by a match at position +6 (fig 3). As *CHRNE* intron 8 has a mismatch at position +6 (fig 1), 857G→T at position −1 probably prevents U1 snRNA from recognising the 5′ splice site of intron 8, and hence causes skipping of exon 8.

To date, 23 splicing mutations of the last nucleotide of an exon have been reported in human to date (table 3). In 17 mutations, the nucleotide at position +6 does not match to U1 snRNA (underlined nucleotides in table 3). In six other mutations that have a matched T nucleotide at position +6, 12 out of 18 nucleotides at positions +3 to +5 are mismatched, whereas in 836 human 5′ splice sites that carry a matched T nucleotide at position +6, only 766 out of 2508 nucleotides are mismatched[17] (Fisher's exact test, $p = 0.003$). These observations also support the idea that a mismatch at position −1 is compensated for by matches at positions +3 to +6, especially at position +6.

Duplication of the 3′ splice site

We constructed and analysed a series of artificial mutants to understand the mechanism by which the duplicated 3′ splice sites resulting from g.IVS10-9_c.1167dup16 silence the downstream copy. Scanning model of recognition of the 3′ splice site indicates that the first "ag" dinucleotide after the branch point is used for splicing catalysis.[8 9] Three exceptions have been reported:[10–12] (*a*) an "ag" dinucleotide less than 13 nucleotides downstream of the branch point is not recognised, probably due to steric effects of *trans* acting elements; (*b*) the first "ag" dinucleotide is hidden in a stable secondary structure; and (*c*) two "ag" dinucleotides that are <12 nucleotides apart compete for being recognised by the splicesome. As the naturally occurring duplication mutant and all artificial mutants except for Mt-Br4 conform to none of the exceptions, they followed the scanning model that favours the first "ag" after the branch point. On the other hand, displacement of a branch point sequence 16 residues downstream (Mt-Br4 in fig 2) placed the "ag" dinucleotide <13 nucleotides downstream of the branch point, and made the upstream copy less competitive than the downstream copy.

Pathogenic duplication of the 3′ splice site has been reported in two other human genes. Both follow the scanning model of recognition of the 3′ splice site. An 18 nucleotide duplication comprising 16 intronic and 2 exonic residues of *HEXB* encoding the β subunit of β-hexosaminidase results in an active upstream copy of the 3′ splice sites.[13] A 69 nucleotide duplication comprising 7 intronic and 62 exonic residues of *SLC4A1* encoding anion exchanger member 1 also results in an active upstream copy of the 3′ splice sites.[14]

Thus, the scanning model of recognition of the 3′ splice site applies to most physiological and pathological duplications of the 3′ splice sites, though exceptions do occur and await explanation.[10 15 16]

Table 3 The 23 previously published splicing mutations at the last nucleotide of an exon

Gene	Exon	Wild type sequence	Mutant nucleotide at −1	Wild type nucleotide at +6
ATM[22]	1	AAGgtagga	A	a
CFTR[23]	2	CAGgtacta	C	a
CPS1[24]	8	AAGgtgcaa	C	a
CYP27[25]	6	GCGgtagga	A	a
FAH[26]	2	CAGgtagga	T	a
HEXA[27]	3	GAGgtaaca	A	a
IL2RG[28]	6	ACGgtgaga	A	a
PKLR[29]	9	GCGgtagga	A	a
PROC[30]	7	CAGgtagga	C	a
COL1A1[31]	6	ATGgtgagc	A	c
COL1A2[32]	6	ATGgtatgc	A	c
COL3A1[33]	3	AAGgtaacc	A	c
CYP27A1[34]	3	AAGgtaccc	C	c
LIPA[35]	8	CAGgtaggc	A	c
LIPA[36]	8	CAGgtaggc	A	c
CDKN2A[37]	2	CAGgtgagg	T	g
UROS[38]	4	AAGgtgagg	T	g
ATM[22]	2	AAGgtatat	A	t
HBB[39]	1	CAGgttggt	C	t
SERPINC1[40]	3	AAGgtgagt	A	t
XPA[41]	3	CAGgtactt	A	t
XPA[41]	4	CAGgtctct	C	t
XPA[42]	5	AAGgtagat	C	t

Nucleotides that do not match to U1 snRNA are underlined, where the matched optimal sequence is "CAGgtaagt". Exonic and intronic nucleotides are indicated by upper and lower case letters, respectively.

ACKNOWLEDGEMENTS

This work was supported by the National Institutes of Health grant NS6277 and by a Muscular Dystrophy Association research grant to A G Engel. We thank Drs Y Harati (patient 2), B Anlar (patient 3), and D Weinberg (patient 5) for patient referral.

Authors' affiliations

K Ohno, A Tsujino, X-M Shen, M Milone, A G Engel, Department of Neurology and Neuromuscular Research Laboratory, Mayo Clinic, Rochester, MN 55905, USA

K Ohno, Division of Neurogenetics and Bioinformatics, Department of Advanced Medical Science, Nagoya University Graduate School of Medicine, 65 Tsurumai, Showa, Nagoya 466-8550, Japan

Competing interests: none declared

Correspondence to: Dr K Ohno, Division of Neurogenetics and Bioinformatics, Department of Advanced Medical Science, Nagoya University Graduate School of Medicine, 65 Tsurumai, Showa, Nagoya 466-8550, Japan; ohnok@med.nagoya-u.ac.jp

Received 20 August 2004
Revised 25 February 2005
Accepted 15 March 2005

REFERENCES

1 **Engel AG**, Ohno K, Sine SM. Neurological diseases: Sleuthing molecular targets for neurological diseases at the neuromuscular junction. *Nat Rev Neurosci* 2003;**4**:339–52.
2 **Barisic N**, Schmidt C, Sidorova OP, Herczegfalvi A, Gekht BM, Song IH, Stucka R, Karcagi V, Abicht A, Lochmuller H. Congenital myasthenic syndrome (CMS) in three European kinships due to a novel splice mutation (IVS7-2A/G) in the epsilon acetylcholine receptor (AChR) subunit gene. *Neuropediatrics* 2002;**33**:249–54.
3 **Croxen R**, Young C, Slater C, Haslam S, Brydson M, Vincent A, Beeson D. End-plate gamma- and epsilon-subunit mRNA levels in AChR deficiency syndrome due to epsilon-subunit null mutations. *Brain* 2001;**124**:1362–72.
4 **Ohno K**, Milone M, Shen XM, Engel AG. A frameshifting mutation in *CHRNE* unmasks skipping of the preceding exon. *Hum Mol Genet* 2003;**12**:3055–66.
5 **Roscigno RF**, Weiner M, Garcia BM. A mutational analysis of the polypyrimidine tract of introns. Effects of sequence differences in pyrimidine tracts on splicing. *J Biol Chem* 1993;**268**:11222–9.
6 **Nakai K**, Sakamoto H. Construction of a novel database containing aberrant splicing mutations of mammalian genes. *Gene* 1994;**141**:171–7.
7 **Berget SM**. Exon recognition in vertebrate splicing. *J Biol Chem* 1995;**270**:2411–14.
8 **Smith CW**, Porro EB, Patton JG, Nadal-Ginard B. Scanning from an independently specified branch point defines the 3′ splice site of mammalian introns. *Nature* 1989;**342**:243–7.
9 **Chen S**, Anderson K, Moore MJ. Evidence for a linear search in bimolecular 3′ splice site AG selection. *Proc Natl Acad Sci USA* 2000;**97**:593–8.
10 **Blasband AJ**, Rogers KT, Chen XR, Azizkhan JC, Lee DC. Characterization of the rat transforming growth factor alpha gene and identification of promoter sequences. *Mol Cell Biol* 1990;**10**:2111–21.
11 **Smith CW**, Chu TT, Nadal-Ginard B. Scanning and competition between AGs are involved in 3′ splice site selection in mammalian introns. *Mol Cell Biol* 1993;**13**:4939–52.
12 **Chua K**, Reed R. The RNA splicing factor hSlu7 is required for correct 3′ splice-site choice. *Nature* 1999;**402**:207–10.
13 **Dlott B**, d'Azzo A, Quon DV, Neufeld EF. Two mutations produce intron insertion in mRNA and elongated beta-subunit of human beta-hexosaminidase. *J Biol Chem* 1990;**265**:17921–7.
14 **Bianchi P**, Zanella A, Alloisio N, Barosi G, Bredi E, Pelissero G, Zappa M, Vercellati C, Baronciani L, Delaunay J, Sirchia G. A variant of the EPB3 gene of the anti-Lepore type in hereditary spherocytosis. *Br J Haematol* 1997;**98**:283–8.
15 **Eller P**, Foger B, Gander R, Sauper T, Lechleitner M, Finkenstedt G, Patsch JR. Wolfram syndrome: a clinical and molecular genetic analysis. *J Med Genet* 2001;**38**:e37.
16 **Penalva LO**, Lallena MJ, Valcarcel J. Switch in 3′ splice site recognition between exon definition and splicing catalysis is important for sex-lethal autoregulation. *Mol Cell Biol* 2001;**21**:1986–96.
17 Ohno K, Brengman JM, Felice KJ, Cornblath DR, Engel AG Congenital end-plate acetylcholinesterase deficiency caused by a nonsense mutation and an A→G splice-donor-site mutation at position+3 of the collagenlike-tail-subunit gene (*COLQ*): How does G at position+3 result in aberrant splicing? *Am J Hum Genet* 1999;**65**:635–44.
18 Ohno K, Quiram PA, Milone M, Wang HL, Harper MC, Pruitt JN 2nd, Brengman JM, Pao L, Fischbeck KH, Crawford TO, Sine SM, Engel AG. Congenital myasthenic syndromes due to heteroallelic nonsense/missense mutations in the acetylcholine receptor ε subunit gene: identification and functional characterization of 6 new mutations, *Hum Mol Genet* 1997;**6**:753–66.
19 **Deymeer F**, Serdaroglu P, Poda M, Gulsen-Parman Y, Ozcelik T, Ozdemir C Clinical characteristic of a group of Turkish patients having a benign CMS phenotype with ptosis and marked ophthalmoparesis and mutations in the acetylcholine receptor epsilon subunit gene. *Acta Myologica* 2000;**19**:29–32.
20 **Ohno K**, Anlar B, Ozdirim E, Brengman JM, DeBleecker JL, Engel AG. Myasthenic syndromes in Turkish kinships due to mutations in the acetylcholine receptor. *Ann Neurol* 1998;**44**:234–41.
21 **Middleton L**, Ohno K, Christodoulou K, Brengman J, Milone M, Neocleous V, Serdaroglu P, Deymeer F, Ozdemir C, Mubaidin A, Horany K, Al-Shehab A, Mavromatis I, Mylonas I, Tsingis M, Zamba E, Pantzaris M, Kyriallis K, Engel AG. Chromosome 17p-linked myasthenias stem from defects in the acetylcholine receptor epsilon-subunit gene. *Neurology* 1999;**53**:1076–82.
22 **Teraoka SN**, Telatar M, Becker-Catania S, Liang T, Onengut S, Tolun A, Chessa L, Sanal O, Bernatowska E, Gatti RA, Concannon P. Splicing defects in the ataxia-telangiectasia gene, ATM: underlying mutations and consequences. *Am J Hum Genet* 1999;**64**:1617–31.
23 **Jones CT**, McIntosh I, Keston M, Ferguson A, Brock DJ. Three novel mutations in the cystic fibrosis gene detected by chemical cleavage: analysis of variant splicing and a nonsense mutation. *Hum Mol Genet* 1992;**1**:11–17.
24 **Hoshide R**, Matsuura T, Haraguchi Y, Endo F, Yoshinaga M, Matsuda I. Carbamyl phosphate synthetase I deficiency. One base substitution in an exon of the CPS I gene causes a 9-basepair deletion due to aberrant splicing. *J Clin Invest* 1993;**91**:1884–7.
25 **Chen W**, Kubota S, Seyama Y. Alternative pre-mRNA splicing of the sterol 27-hydroxylase gene (CYP 27) caused by a G to A mutation at the last nucleotide of exon 6 in a patient with cerebrotendinous xanthomatosis (CTX). *J Lipid Res* 1998;**39**:509–17.
26 **Rootwelt H**, Berger R, Gray G, Kelly DA, Coskun T, Kvittingen EA. Novel splice, missense, and nonsense mutations in the fumarylacetoacetase gene causing tyrosinemia type 1. *Am J Hum Genet* 1994;**55**:653–8.
27 **Ozkara HA**, Sandhoff K. A new point mutation (G412 to A) at the last nucleotide of exon 3 of hexosaminidase alpha-subunit gene affects splicing. *Brain Devt* 2003;**25**:203–6.
28 **Kanai N**, Yanai F, Hirose S, Nibu K, Izuhara K, Tani T, Kubota T, Mitsudome A. A G to A transition at the last nucleotide of exon 6 of the gamma c gene (868G→A) may result in either a splice or missense mutation in patients with X-linked severe combined immunodeficiency. *Hum Genet* 1999;**104**:36–42.
29 **Kanno H**, Fujii H, Wei DC, Chan LC, Hirono A, Tsukimoto I, Miwa S. Frame shift mutation, exon skipping, and a two-codon deletion caused by splice site mutations account for pyruvate kinase deficiency. *Blood* 1997;**89**:4213–18.
30 **Lind B**, van Solinge WW, Schwartz M, Thorsen S. Splice site mutation in the human protein C gene associated with venous thrombosis: demonstration of exon skipping by ectopic transcript analysis. *Blood* 1993;**82**:2423–32.
31 **Weil D**, D'Alessio M, Ramirez F, de Wet W, Cole WG, Chan D, Bateman JF. A base substitution in the exon of a collagen gene causes alternative splicing and generates a structurally abnormal polypeptide in a patient with Ehlers-Danlos syndrome type VII. *EMBO J* 1989;**8**:1705–10.
32 **Weil D**, D'Alessio M, Ramirez F, Steinmann B, Wirtz MK, Glanville RW, Hollister DW. Temperature-dependent expression of a collagen splicing defect in the fibroblasts of a patient with Ehlers-Danlos syndrome type VII. *J Biol Chem* 1989;**264**:16804–9.
33 **Kuivaniemi H**, Tromp G, Bergfeld WF, Kay M, Helm TN. Ehlers-Danlos syndrome type IV: a single base substitution of the last nucleotide of exon 34 in COL3A1 leads to exon skipping. *J Invest Dermatol* 1995;**105**:352–6.
34 **Garuti R**, Lelli N, Barozzini M, Tiozzo R, Dotti MT, Federico A, Ottomano AM, Croce A, Bertolini S, Calandra S. Cerebrotendinous xanthomatosis caused by two new mutations of the sterol-27-hydroxylase gene that disrupt mRNA splicing. *J Lipid Res* 1996;**37**:1459–67.
35 **Klima H**, Ullrich K, Aslanidis C, Fehringer P, Lackner KJ, Schmitz G. A splice junction mutation causes deletion of a 72-base exon from the mRNA for lysosomal acid lipase in a patient with cholesteryl ester storage disease. *J Clin Invest* 1993;**92**:2713–18.
36 **Aslanidis C**, Ries S, Fehringer P, Buchler C, Klima H, Schmitz G. Genetic and biochemical evidence that CESD and Wolman disease are distinguished by residual lysosomal acid lipase activity. *Genomics* 1996;**33**:85–93.
37 Rutter JL, Goldstein AM, Davila MR, Tucker MA, Struewing JP CDKN2A point mutations D153spl(c.457G→T) and IVS2+1G→T result in aberrant splice products affecting both p16INK4a and p14ARF. *Oncogene* 2003;**22**:4444–8.
38 **Xu W**, Astrin KH, Desnick RJ. Molecular basis of congenital erythropoietic porphyria: mutations in the human uroporphyrinogen III synthase gene. *Hum Mutat* 1996;**7**:187–92.
39 **Vidaud M**, Gattoni R, Stevenin J, Vidaud D, Amselem S, Chibani J, Rosa J, Goossens M. A 5′ splice-region G→C mutation in exon 1 of the human beta-globin gene inhibits pre-mRNA splicing: a mechanism for beta+-thalassemia. *Proc Natl Acad Sci USA* 1989;**86**:1041–5.
40 **Berg LP**, Grundy CB, Thomas F, Millar DS, Green PJ, Slomski R, Reiss J, Kakkar VV, Cooper DN. De novo splice site mutation in the antithrombin III (AT3) gene causing recurrent venous thrombosis: demonstration of exon skipping by ectopic transcript analysis. *Genomics* 1992;**13**:1359–61.
41 **Satokata I**, Tanaka K, Yuba S, Okada Y. Identification of splicing mutations of the last nucleotides of exons, a nonsense mutation, and a missense mutation of the XPAC gene as causes of group A xeroderma pigmentosum. *Mutat Res* 1992;**273**:203–12.
42 **Sato M**, Nishigori C, Yagi T, Takebe H. Aberrant splicing and truncated-protein expression due to a newly identified XPA gene mutation. *Mutat Res* 1996;**362**:199–208.

doi:10.1093/brain/awh364 *Brain* (2005), **128**, 345–355

Subunit-specific contribution to agonist binding and channel gating revealed by inherited mutation in muscle acetylcholine receptor M3–M4 linker

Xin-Ming Shen,[1] Kinji Ohno,[1] Steven M. Sine[2] and Andrew G. Engel[1]

[1]*Department of Neurology and Neuromuscular Research Laboratory and* [2]*Department of Physiology and Biophysics and Receptor Biology Laboratory, Mayo Clinic, Rochester, MN, USA*

Correspondence to: Dr Andrew G. Engel, Department of Neurology, Mayo Clinic, 200 First Street SW, Rochester, MN 55905, USA
E-mail: age@mayo.edu

Summary

We trace the cause of congenital myasthenic syndromes in two patients to mutations in the ε subunit of the muscle acetylcholine receptor (AChR). Both patients harbour deletion of an asparagine residue in the ε subunit (εN436del) at the C-terminus of the cytoplasmic loop linking the third (M3) and fourth (M4) transmembrane domains. The presence of a null mutation in the second allele of the ε subunit shows that εN346del determines the phenotype. Endplate studies show markedly reduced expression of the εN346del-AChR and compensatory accumulation of fetal γ-AChR. Expression studies in HEK cells reveal decreased expression of εN436del-AChR and abnormally brief channel openings. Thus, neuromuscular transmission is compromised by AChR deficiency, fast channel kinetics of the εN346del-AChR and incomplete phenotypic rescue by γ-AChR. Single-channel kinetic analysis shows that the εN436del shortens channel openings by reducing stability of the diliganded receptor: rates of channel closing and of ACh dissociation are increased and the rate of channel opening is decreased. In addition to shortening the M3–M4 loop, εN436del shifts a negatively charged aspartic acid residue adjacent to M4; the effects of εN436del are shown to result from shortening of the M3–M4 loop and not from juxtaposition of a negative charge to M4. To determine whether the consequences of εN346del are subunit-specific, we deleted residues that align with εN436 in β, δ and α subunits. Each deletion mutant reduces AChR expression, but whereas the β and δ mutants curtail channel open duration, the α mutant strikingly prolongs open duration. Kinetic analysis reveals that the α mutant increases the stability of the diliganded receptor: rates of channel closing and of ACh dissociation are decreased and the rate of channel opening is increased. The overall studies reveal subunit asymmetry in the contributions of the M3–M4 loops in optimizing AChR activation through allosteric links to the channel and the agonist binding site.

Keywords: acetylcholine receptor; congenital myasthenic syndrome; M3–M4 loop; mutagenesis; single-channel patch-clamp recordings

Abbreviations: ACh = acetylcholine; AChR = acetylcholine receptor; α-bgt = α-bungarotoxin; CMS = congenital myasthenic syndrome; EP = endplate; HEK = human embryonic kidney; M = transmembrane domain; MEPC = miniature endplate current

Received August 12, 2004. Revised November 4, 2004. Accepted November 5, 2004. Advance Access publication December 22, 2004

Introduction

The nicotinic acetylcholine receptor (AChR) at the motor endplate (EP) is a heteropentamer of homologous subunits with stoichiometries $\alpha_2\beta\delta\varepsilon$ for the adult-type receptor and $\alpha_2\beta\gamma\delta$ for the fetal type. Each subunit contains four transmembrane domains and short (M1–M2) and long (M3–M4) cytoplasmic loops. The M3–M4 loops of the subunits constitute most of the cytoplasmic mass of AChR (Popot and Changeux, 1984) and harbour three predicted amphipathic helices (Le Novère *et al.*, 1999), one of which borders M4. The M3–M4 loops regulate the flow of ions through the channel (Miyazawa *et al.*, 1999) and affect the rate of channel closing; structural differences between the loops of the γ and ε

subunits are major determinants of the change from fetal to adult AChR kinetics (Bouzat *et al.*, 1994). The M3–M4 loops also interact with rapsyn to cluster AChR at the EP, but the residues that bind the receptor to rapsyn have not been determined (Gensler *et al.*, 2001; Huebsch and Maimone, 2003; Maimone and Merlie, 1993; Yu and Hall, 1994).

Congenital myasthenic syndromes (CMS) are heterogeneous disorders caused by defects in presynaptic, synaptic basal lamina or postsynaptic gene products (Engel *et al.*, 2003). Most CMS are postsynaptic, and most postsynaptic CMS are caused by mutations in AChR subunits (Engel *et al.*, 2003). To date, six missense mutations have been observed in the M3–M4 loops. An in-frame duplication of residues 413–418 (ε1254ins18) (Milone *et al.*, 1998) and a missense mutation (εA411P) (Wang *et al.*, 2000), both in the amphipathic helix of the ε subunit, corrupt the fidelity of gating and result in irregular channel kinetics. A three-codon deletion of residues 426–428 of the β subunit (β426EQEdel) disrupts a specific interaction between the β and δ subunits and impairs AChR assembly (Quiram *et al.*, 1999). Three missense mutations [εR311W (Ohno *et al.*, 1997), εP331L (Croxen *et al.*, 2001) and αV402F (Milone *et al.*, 1999)] reduce surface expression of AChR. Additionally, εR311W mildly shortens and αV402F modestly prolongs channel opening events.

Here we trace the cause of a myasthenic syndrome in two patients to two heteroallelic mutations in the acetylcholine receptor (AChR) ε subunit: deletion of the C-terminal residue of the M3–M4 cytoplasmic loop (εN436del) plus a null mutation in the second ε allele. When εN436del-AChR and corresponding deletion mutants of other AChR subunits are expressed in human embryonic kidney (HEK) cells, each mutant reduces AChR expression, but whereas the ε, β and δ deletion mutants decrease, the α deletion mutant markedly increases the duration of channel opening episodes. Kinetic analysis reveals that the ε deletion mutant has decreased ACh affinity for the diliganded closed state and impaired gating efficiency, whereas the α deletion mutant markedly enhances ACh affinity and gating efficiency. Thus, the presence of the C-terminal residue of each M3–M4 loop is essential for normal expression, and loops from the different subunits contribute in an asymmetrical manner to optimize activation of AChR.

Methods

Muscle specimens

Intercostal muscle specimens were obtained intact from origin to insertion from patients and control subjects without muscle disease undergoing thoracic surgery. All human studies were in accord with the guidelines of the Institutional Review Board of the Mayo Clinic.

AChR and acetylcholinesterase were detected in cryostat sections by two-colour fluorescence (Hutchinson *et al.*, 1993). Endplates (EPs) were localized for electron microscopy and analysed by the established methods (Engel 1994*a*, *b*). Peroxidase-labelled α-bungarotoxin (α-bgt) was used for the ultrastructural localization of AChR (Engel *et al.*, 1977). The number of AChRs per EP was measured with [^{125}I]α-bgt (Engel *et al.*, 1993).

Electrophysiology of muscle specimens

Recordings of miniature EP currents and estimates of the number of transmitter quanta released by nerve impulse were carried out as described elsewhere (Engel *et al.*, 1993; Uchitel *et al.*, 1993). Single-channel patch-clamp recordings from EP AChR were performed in the cell-attached mode as previously described (Milone *et al.*, 1994).

Mutation analysis

We directly sequenced the AChR ε subunit gene using genomic DNA (Ohno *et al.*, 1996). For family analysis, we traced the εIVS9-1G→C mutation by *Eco*NI and the ε911delT mutation by *Eco*72I restriction analysis of PCR products. The εN436del mutations was traced with allele-specific PCR in family members and in 200 normal alleles of 100 unrelated controls.

Construction and expression of wild-type and mutant AChRs

Sources of human α, β, ε and δ subunit cDNAs were as previously described (Luther *et al.*, 1989; Ohno *et al.*, 1996; Schoepfer *et al.*, 1988). All four cDNAs were subcloned into the CMV-based expression vector pRBG4 (Sine, 1993) for expression in human embryonic kidney fibroblast (293 HEK) cells. The artificial mutations were engineered into wild-type AChR subunit cDNAs in pRBG4 using the QuikChange Site-Directed Mutagenesis Kit (Stratagene). The presence of each mutation and the absence of unwanted mutations was confirmed by sequencing the entire inserts. HEK cells were transfected with a total of 7.2 μg of plasmids, comprising pRBG4-α, -β, -δ, -ε and pEGFP-N1 in a ratio of 2 : 1 : 1 : 1 : 1 per 35 mm dish using the calcium phosphate precipitation method (Bouzat *et al.*, 1994; Ohno *et al.*, 1996), or a total of 2 μg of plasmids using 6 μl of the FuGene6 transfection reagent (Roche). For patch-clamp studies, we enhanced expression of εDN435del-, αH408del-, βR446del-, δR450del-, β-omitted and δ-omitted AChRs by adding 1 μg of the pAdVAntage plasmid (Promega) per 10 μg of total AChR subunit cDNAs.

Bungarotoxin binding measurements

The total number of [^{125}I]α-bgt sites on the surface of transfected human embryonic kidney (HEK) cells and ACh competition against the initial rate of [^{125}I]α-bgt binding were determined as described elsewhere (Ohno *et al.*, 1996). ACh competition measurements were analysed using the monophasic Hill equation for wild-type and εN436del-AChR (Equation 1) or the two-binding-site equation for ε-omitted AChR (Equation 2):

$$1 - Y = 1/(1 + ([ACh]/K_{ov})^n) \quad (1)$$

$$1 - Y = \text{fract}_A/(1 + [ACh]/K_A) + (1 - \text{fract}_A)/(1 + [ACh]/K_B) \quad (2)$$

where Y is fractional occupancy by ACh, n is the Hill coefficient, K_{OV} is an overall dissociation constant, K_A and K_B are the dissociation constants for the two binding sites, and fract_A is the fraction of sites with dissociation constant K_A.

Patch-clamp recordings from AChRs expressed in HEK cells

Recordings were obtained in the cell-attached configuration at a membrane potential of −80 mV, at 22°C, and with bath and pipette solutions containing (mM): KCl 142, NaCl 5.4, $CaCl_2$ 1.8, $MgCl_2$ 1.7,

HEPES 10, pH 7.4 (Bouzat *et al.*, 1994; Ohno *et al.*, 1996). Single-channel currents were recorded using an Axopatch 200A amplifier (Axon Instruments) at a bandwidth of 50 kHz, digitized at 5 μs intervals using a Digidata 1200A (Axon Instruments), and recorded to hard disk using the program Clampex 8 (Axon Instruments). Records were analysed at a uniform bandwidth of 11.7 kHz with TACx4.0.9 software (Bruxton). Dwell-time histograms were plotted on a logarithmic abscissa and fitted to the sum of exponentials by maximum likelihood (Sigworth and Sine, 1987).

To estimate rate constants underlying AChR activation, we employed desensitizing concentrations of ACh that cause events from a single channel to cluster into identifiable activation episodes (Qin *et al.*, 1996). Clusters were identified as a series of closely spaced openings preceded and followed by closed intervals greater than a defined critical time. The critical time was determined by a method that misclassifies an equal number of events between two adjacent closed-time components (Colquhoun and Sakmann, 1985). For each receptor, the critical time that provided the best fit for the closed time histogram was chosen for the final analysis. Clusters with fewer than five openings were excluded from analysis. Individual clusters were examined for homogeneity by determining the mean open probability and open duration for each cluster, and clusters within two standard deviations of the means were accepted for further analysis (Qin *et al.*, 1996; Shen *et al.*, 2003). The resulting open and closed intervals were analysed according to kinetic schemes of receptor activation using the program MIL, which uses an interval-based maximum likelihood method that also corrects for missed events (Qin *et al.*, 1996). A dead time of 23 μs was imposed on all recordings. For each type of AChR, single-channel dwell times obtained at a range of ACh concentrations were fitted simultaneously. Data for wild-type AChR were obtained at 10, 20, 30, 50, 70, 100, 200 and 300 μM ACh, for εN436del-AChR at 20, 30, 50, 70, 100, 200 and 300 μM ACh, and for αH408del-AChR at 0.3, 1, 3 and 10 μM ACh. An average of 8900 events were analysed for each ACh concentration with the range from 1867 to 15 500. The final set of rate constants were checked by superimposing probability density functions calculated from the rate constants on the experimental dwell time histograms, and by their ability to predict burst length at low ACh concentrations (Colquhoun and Sigworth, 1995; Colquhoun and Hawkes, 1995).

Results

Characteristics of CMS patients

Patient 1, a 25-year-old woman (Fig. 1A), and patient 2, a 12-year-old-girl, had severe myasthenic symptoms since birth, a decremental compound muscle action potential response on repetitive stimulation of motor nerves at 2 Hz, and negative tests for anti-AChR antibodies. Both patients responded partially to pyridostigmine and improved further with the additional use of 3,4-diaminopyridine. The parents are not consanguineous, and there are no similarly affected relatives.

Endplate studies

The configuration of the EPs, evaluated from the cytochemical reaction for acetylcholinesterase on teased muscle fibres, was abnormal, with an increased number of small EP regions (1–10 in patient 1 and 2–8 in patient 2) distributed over an increased span of the muscle fibre surface. The number of

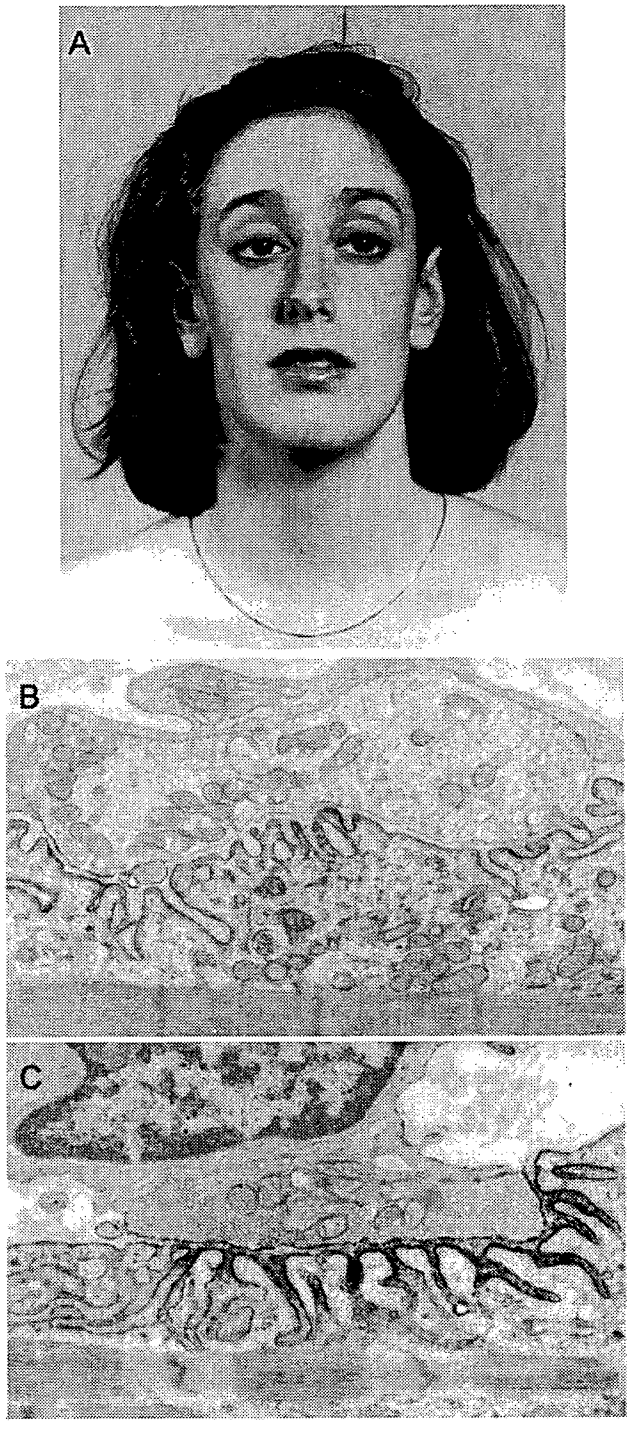

Fig. 1 (A) Patient 1 at age 25 shows ptosis, hyperactive frontalis muscle, mild exotropia, lack of facial expression, elongated face, and large ears. AChR is localized at patient (**B**) and control (**C**) EP regions with peroxidase-labelled α-bgt. The patient EP has a simplified postsynaptic region and attenuated reaction for AChR. Magnification, ×26 000.

[^{125}I]α-bgt binding sites per EP was ~10% of normal (Table 1). Electron microscopy examination of 16 EPs in patient 1 (Fig. 1B and C) and 24 EPs in patient 2 showed a decreased density and restricted distribution of AChR on the junctional folds. The integrity of the junctional folds and

Table 1 *Endplate studies*

	Patient 1	Patient 2	Controls
^{125}I α-bgt binding sites/EP	1.20 E6	1.27 E6	12.82 ± 0.79 E6
EPP quantal content (1 Hz)[a]	51 ± 3 (25)	46 ± 6 (15)	31 ± 1 (190)
MEPC amplitude (nA)[b]	1.34 ± 0.05 (17)	1.74 ± 0.12 (15)	3.95 ± 0.10 (79)
τ_{MEPC} (ms)[b,c]	6.35 ± 0.32 (17)		3.23 ± 0.06 (79)
	(ii) 1.03 ± 0.11 (15)	(i) 0.90 ± 0.09 (13)	
	(ii) 9.30 ± 0.66 (15)	(ii) 5.80 ± 0.66 (13)	
Burst duration of 60 pS channels[d]			
τ_1 (ms)	ND	0.053 ± 0.0068 (5)	0.090 ± 0.03 (7)
Area		(0.23 ± 0.036)	(0.13 ± 0.02)
τ_2 (ms)	ND	0.85 ± 0.063 (5)	2.99 ± 0.26 (7)
Area		(0.77 ± 0.063)	(0.87 ± 0.02)

Values represent mean ± SEM; numbers in parentheses indicate number of EPs, except for [^{125}I]α-bgt binding sites/EP, where they indicate number of control subjects. T = 29 ± 0.5°C for EPP recordings, and 22 ± 0.5°C for MEPC and patch-clamp recordings. ND = not detected. [a]Quantal content of EP potential (EPP) at 1 Hz stimulation corrected for resting membrane potential of −80 mV, non-linear summation, and non-Poisson release. [b]−80 mV. [c]In patient 1, monoexponentially decaying MEPCs were recorded from 17 EPs; at 15 of these EPs biexponentially decaying MEPCs were also present. In patient 2, all MEPCs at all EPs decayed biexponentially. [d]ACh, 1 μM; pipette potential, 80 mV; bandwidth, 12 kHz.

nerve terminals was preserved but some postsynaptic regions were simplified (Fig. 1B). Quantal release by nerve impulse was higher than normal (Table 1), probably as an adaptive response to decreased postsynaptic sensitivity to ACh (Plomp *et al.*, 1992, 1995). The miniature EP current (MEPC) amplitude was reduced to 34% of normal in patient 1 (Fig. 1A) and to 44% of normal in patient 2. In patient 1, most MEPCs observed at 17 EPs decayed abnormally slowly and were best fitted by a single exponential, but a small proportion of the EPs (11%) at 15 of the 17 EPs was best fitted by two exponentials, with one component shorter and one component three times longer than normal (Table 1 and Fig. 2A). In patient 2, MEPCs recorded from all 13 EPs decayed biexponentially, with one component shorter and the other twice longer than normal (Table 1).

Single-channel recordings from EPs of patient 2 showed that most channels opened to a low conductance (~40 pS) and had long burst open durations characteristic of fetal-type γ-AChRs (Fig. 2B), but a small proportion (6%) of channels opened to the ~60 pS conductance of adult-type ε-AChRs and had shorter than normal burst durations (Table 1). To summarize, EP studies revealed AChR deficiency, expression of fetal γ-AChR, and abnormally brief activation episodes of the expressed adult ε-AChR.

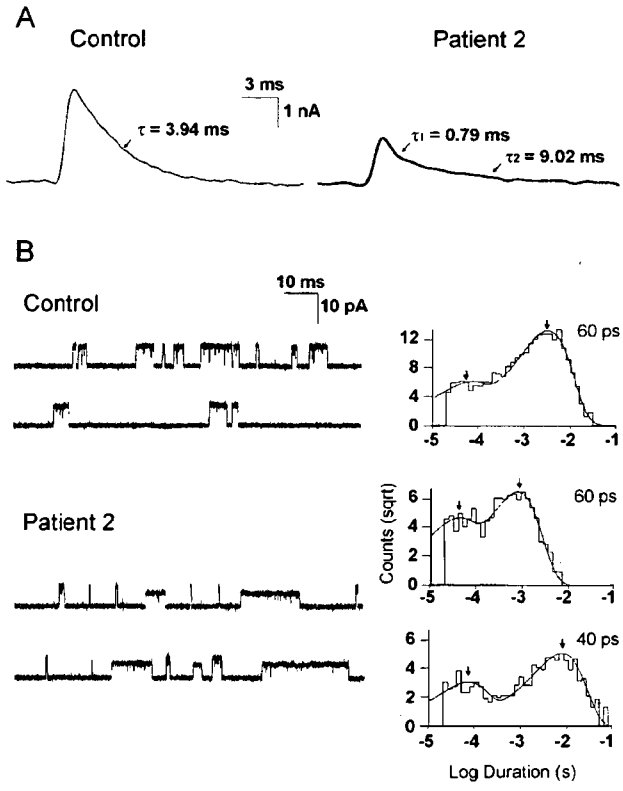

Fig. 2 (**A**) MEPCs recorded from a control (*left*) and patient 2 (*right*) EPs. Arrows indicate MEPC decay time constants. The patient MEPC has a lower amplitude and decays more slowly than the control MEPC. Patient MEPC represents an average of 34 traces; the control MEPC represents the average of 64 traces. (**B**) (*Left*) AChR channel events recorded from a control EP and from EP of patient 2. Openings are shown as upward deflections. ACh = 1 μM. At patient EP, note prolonged low-amplitude channel openings characteristic of fetal γ-AChR and brief higher-amplitude channel openings of adult AChR. (*Right*) Burst duration histograms fitted to the sum of exponentials at control EP, and for 60 pS and 40 pS channel openings at patient EP. Arrows indicate mean durations of burst components. Bandwidth, 12 kHz; membrane potential, −80 mV; temperature, 22 ± 0.5°C.

Mutation analysis

To examine the genetic basis of the observed morphological and physiological abnormalities, we directly sequenced the AChR ε subunit gene and detected three mutations in the two patients (Fig. 3D). Both patients have a 3-bp deletion (ε1306delAAC) in ε exon 12 that predicts deletion of an asparagine residue at the C-terminus of the M3–M4 loop of the ε subunit (εN436del). The deleted asparagine at codon 436 is conserved in the mouse and rat but not in the *Xenopus* or bovine ε subunit or in other human subunits (Fig. 3A). εN436del was not observed in 200 normal alleles.